Journal of ELECTRONIC MATERIALS, Vol. 43, No. 6, 2014
DOI: 10.1007/s11664-014-3020-x

Analysis of Thermoelectric Generator Performance by Use of Simulations and Experiments

OLLE HÖGBLOM[1] and RONNIE ANDERSSON[1,2]

1.—Department of Chemical and Biological Engineering, Chalmers University of Technology, 41296 Göteborg, Sweden. 2.—e-mail: ronnie.andersson@chalmers.se

A method that enables accurate determination of contact resistances in thermoelectric generators and which gives detailed insight into how these reduce module performance is presented in this paper. To understand the importance taking thermal and electrical contact resistances into account in analysis of thermoelectric generators, full-scale modules were studied. Contact resistances were determined by means of non-linear regression analysis on the basis of results from 3D finite element simulations and experiments in a setup in which heat flow, voltage, and current were measured. Statistical evaluation showed that the model and the identified contact resistances enabled excellent prediction of performance over the entire range of operating conditions. It was shown that if contact resistances were not included in the analysis the simulations significantly over-predicted both heat flow and electric power output, and it was concluded that contact resistance should always be included in module simulations. The method presented in this paper gives detailed insight into how thermoelectric modules perform in general, and also enables prediction of potential improvement in module performance by reduction of contact resistances.

Key words: Thermoelectric modeling, thermal contact resistance, electrical contact resistance

Nomenclature

c_p Specific heat capacity, J kg^{-1} K^{-1}
I Current, A
J Current density, A m^{-2}
P Electric power, W
Q Heat flow, W
SS Normalized sum of squares error
T Temperature, K
U Voltage, V

Greek symbols

α Seebeck coefficient, V K^{-1}
β Thermal contact resistance, m^2 K W^{-1}
γ Electric contact resistance, Ω m^2
λ Thermal conductivity, W m^{-1} K^{-1}
ρ Density, kg m^{-3}
σ Electric conductivity, Ω^{-1} m^{-1}

Subscripts

c Cold side
h Hot side

(Received June 30, 2013; accepted January 9, 2014; published online February 4, 2014)

INTRODUCTION

The development of thermoelectric (TE) devices, for example thermoelectric generators (TEG) and thermoelectric coolers (TEC), relies to a large extent on simulation tools that predict performance. For this purpose several studies have been conducted to evaluate the accuracy of different modeling approaches proposed in the literature.[1,2] The models proposed in the literature range from simplified macroscopic models based on the global balance of heat transfer and thermoelectric effects, to three-dimensional simulations based on the finite element method (FEM) that take into account all relevant thermoelectric phenomena, i.e. Seebeck, Peltier, Thomson, and Joule effects.[3] Thermoelectric simulations based on FEM are becoming widespread, because they provide detailed information about potential, current flow, and temperature distribution within TE modules and readily enable details of geometry and non-linear material properties to be taken into account. When performing FEM simulations of complete TE modules several unknown properties related to the characteristics of the modules must be determined to complete the model. These include thermal and electrical conductance at different material junctions inside the modules. Whereas the properties of the bulk material, e.g. the Seebeck coefficient, thermal conductivity, and electric resistivity, and their temperature dependence, depend on the choice of n-type and p-type material, thermal conductance, i.e. the inverse of thermal resistance, at interfaces depends on material properties, surface roughness, and applied contact pressure.[4] Consequently the thermal conductances of the different material junctions inside the modules vary substantially. Values between 2×10^{3} W m^{-2} K^{-1} and 1×10^{6} W m^{-2} K^{-1} are reported in the literature; these correspond to contact resistance in the range 1×10^{-6}–5×10^{-4} m^{2} KW^{-1}, depending on the specific material junctions. These interfacial resistances can be compared with the thermal resistance of the bulk materials, to assess whether or not they can be neglected. An estimate of the thermal resistance of the bulk is $\beta_{\text{bulk}} = L/\lambda$. The pellets inside TE modules are of the order of 1 mm, and the thermal conductivity of the bulk material is typically 2 Wm^{-1} K^{-1}. Consequently, the thermal resistance of the bulk material is approximately 5×10^{-4} m^{2} KW^{-1}. This means the interfaces may result in substantial resistance to heat transfer compared with the resistance of the bulk material; they can, therefore, have a substantial effect on temperature profile, heat flow, and, thus, module performance. Ziolkowski et al.[5] have used simulations to study contact resistances within TEG and observed negligible thermal resistance between the pellets and the contact bridges. However, in their research they did not investigate the other thermal contact resistances present inside a TE module.

Similarly, material junctions also result in electrical contact resistances. Ziolkowski reports contact resistances in the range 1×10^{-9}–1×10^{-7} Ωm^{2}, depending on production conditions. Assuming a 1-mm pellet with electrical resistivity of 1×10^{-5} Ωm, the electrical resistance of the pellet is approximately 1×10^{-8} Ωm^{2}. Therefore, electrical contact resistances must be determined to enable system-level simulations of TEG modules.

Consequently, neither thermal nor electrical contact resistances should be neglected when performing TEG module simulations. Because contact resistances can, potentially, have a large effect on TEG module simulations, contact resistances inside the module should be characterized. To this end, in this paper a system-level analysis of thermal and electrical contact resistances, how these can be determined accurately, and the effect they have on simulation of TEG performance is reported.

METHODOLOGY

The experimental measurement setup used in this research enabled highly accurate determination of voltage, current, and heat flow through TEG modules exposed to different thermal gradients. An FEM model of the thermoelectric generator, including thermal and electrical contact resistances, was subsequently built and simulated by use of Ansys. Simulations were performed for the same operating conditions as in the experiments, and the contact resistances inside the module were identified by use of non-linear regression analysis. Finally the identified contact resistances were used to predict the performance of a geometrically different module, manufactured by use of the same process and made of the same materials, to assess the consistency of the model and the measured contact resistances.

EXPERIMENTAL SETUP

To characterize module performance in terms of heat flow, electric voltage, and current a setup enabling the dependent variables to be measured with high accuracy is required. For this purpose the symmetric experimental setup shown in Fig. 1a was used. It consisted of one electrically heated aluminium block in the center, with one thermoelectric module on each side of the block. By measuring the performance of two modules operating under the same conditions, potential variability between the modules could be identified. Experimental data showed that both modules gave identical performance for the same temperature difference. The high thermal conductivity of aluminium ensures even temperature distribution throughout the hot block and, thus, over the module surface. The temperatures were measured with thermocouples inside the hot block. Measurements at different locations inside the hot block showed that the temperature variation was below 1°C, which is insignificant and enables use of constant temperature boundary conditions in the simulations.

Water-cooled aluminium blocks were used as heat sinks on the cold side of the modules. Because the water was heated on its way through the system, the water channels in the blocks were connected in series, from one block to the other and back again, so the temperature distribution was as uniform as possible. The mass flow rate of water affected the temperature difference between the two cold blocks, i.e. the higher the mass flow rate of water, the lower the temperature difference between the blocks. Temperature measurements with thermocouples inside the cold blocks confirmed that variation between the two blocks was below 2°C, which is low compared with the temperature difference between the cold and hot blocks (in the range 60–150°C) in the experiments, Table I.

The heat flow through the modules was calculated from the energy balance, on the basis of measured mass flow rates of cooling water and the inlet and outlet water temperatures in the setup. Consequently, the maximum mass flow rate of cooling water that could be used to minimize the temperature difference between the two cold blocks was limited by the accuracy of measurement of the inlet and outlet water temperatures. The energy balance was possi-

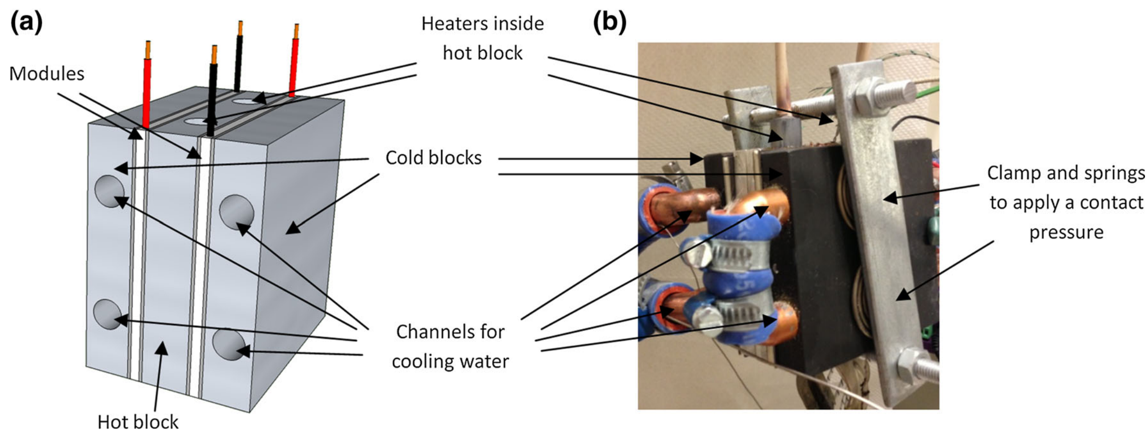

Fig. 1. (a) Schematic diagram of the measurement setup. (b) Photograph of the setup.

Table I. Measurement data for the large module, TEHP1-12680-0.15

Load point	T_h (°C)	T_c (°C)	U (V)	I (A)	Q (W)	P (W)
1	111	50	0.89	3.13	202	2.8
2	127	56	1.07	3.53	239	3.8
3	140	60	1.22	3.90	271	4.8
4	158	65	1.33	4.26	311	5.7
5	171	69	1.55	4.71	354	7.3
6	179	62	1.74	5.22	419	9.1
7	192	66	1.92	5.49	457	10.5
8	207	71	2.07	5.88	507	12.2
9	225	76	2.27	6.06	547	13.8

bly affected by convection and radiation from the cold blocks. Experiments were performed to determine the heat losses by wrapping the cold block with insulating material (Superwool 607 HT; Morgan Advanced Materials, UK; thermal conductivity of 0.08 $Wm^{-1} K^{-1}$) 2 cm. The results showed that losses were below 1% in the operating range of interest.

The cold blocks were held together with a clamp and two springs to achieve the specified contact pressure for these modules. A photograph of the hardware is shown in Fig. 1b. The two modules studied here were commercial bismuth telluride modules from Thermonamic. The first module, TEHP1-12680-0.15, was 80 mm × 80 mm and consisted of 126 TE pairs; hereinafter this will be referred to as the "large module". The second module, TEP1-1264-1.5, was 40 mm × 40 mm and contained 127 TE pairs; this will be referred to as the "small module". The dimensions of the pellets and the connecting bridges and their arrangement inside the modules were determined by opening the modules, thus enabling measurement of interior parts.

The thermoelectric module was connected in series with an electronic load, TTI LD300 (Thurlby Thandar Instruments, UK), so the external resistance was approximately 0.3 ohm for the large module and approximately 3 ohm for the small module. The resistance was slightly varied at each load point to achieve a voltage over the module that was 50% of the voltage when it was measured at open circuit at the same temperature. This was done to maximize the power delivered by the modules. The hot-side temperature was incremented in nine steps and all the measurements were taken when steady state conditions were achieved. Data were sampled by use of a DataTaker DT85 (Thermo Fisher Scientific, Australia).

MODEL DESCRIPTION

The thermoelectric modules consisted of several small thermocouples connected electrically in series and thermally in parallel, as shown schematically in Fig. 2. The external surfaces of the modules were covered with a thin layer of graphite that had to be compressed to reduce the thermal resistance. A graphite layer also covered the interior of the modules, between the connecting bridges on the hot side and the ceramic plate (red in Fig. 2). The connecting bridges were soldered to the pellets on the cold side and the bridges on the hot side were formed directly on the pellets by thermal spraying.

The unknown contact resistances included the electrical contact resistances, on both sides of the thermoelectric pellets, and the thermal contact resistances between the pellets and the connectors, and between the connectors and the ceramic plates (Fig. 2). In other words, there were 504 electrical resistances in series and four thermal resistances in series inside the large module. In this work the In this work three contact resistances were used—two thermal contact resistances, one on each side of the module, and one electrical contact resistance. The thermal contact resistances in the model were applied to the surface between the ceramic plate and the connecting bridges, as shown in Fig. 2. There were also thermal contact resistances between the thermoelectric pellets and the connecting bridges, but, because it is the temperature on the surface of the thermoelectric material that is of interest in generation of thermoelectricity, these resistances were grouped together. The electrical resistances were assumed to be the same on the hot and the cold sides, and for the n-type and p-type materials. This is a valid assumption, because the sum of all the electrical resistances is what is important here. The resistances were also assumed not to have any temperature dependence.

In thermoelectric calculations the temperature field inside the thermoelectric module, the electric charge continuity equation, and the thermoelectric constitutive equations enable calculation of the current and voltage.[6] The energy equation solved for the thermoelectric material consists of, in addition to the conduction and accumulation terms, two terms describing ohmic heating and thermoelectric conversion (Eq. 1):

$$-\nabla(\lambda\nabla T) = \rho c_{\mathrm{p}}\frac{\partial T}{\partial t} + \frac{J^2}{\sigma} + \nabla\alpha TJ. \qquad (1)$$

The potential field is built up by diffusion of the charge carrier in the direction of the temperature gradient and is reduced by ohmic losses, in accordance with Eq. 2:

$$\nabla U = -\alpha\nabla T - J/\sigma. \qquad (2)$$

In addition to the contact resistances and the constitutive equation above, boundary conditions are needed to solve the model. The boundary condition for the potential field calculations is a cross section of the electric connector that is electrically grounded. The two boundary conditions used when solving the energy equation are identical to the two temperatures measured in the aluminium blocks. For this reason, the thermal resistance in the outer graphite layer on the modules is included in the analysis, which is necessary for system-level simulations. The simulation model is shown in Fig. 3 where the external load is encircled. During the simulations the load was kept at a constant temperature, to prevent it being heated, which would have affected the heat flow in the module. The resistance was varied by assigning different resistivity to the load in accordance with the external load used in the measurements. The geometry of the thermoelectric module was discretized with hexahedral elements, and a grid sensitivity analysis was performed to ensure grid independence in the simulations.

Thermoelectric simulations require relevant material data, for example the Seebeck coefficient, electrical resistivity, and thermal conductivity. Temperature-dependent material data for the bismuth telluride used in the modules was obtained from the manufacturer,[7] and is shown in Fig. 4. The connecting bridges inside the modules were made of copper on the cold side and aluminium on the hot side. The ceramic plates enclosing the module were made of aluminium oxide. The temperature dependence of all these materials was also included in the model.

RESULTS

Experiments were conducted under nine different operating conditions; the measured data at these different load points is summarized in Table I. Simulations were performed at identical temperatures and external load, as in the experiments. Each load point had three dependent variables; current, voltage, and heat flow. This means that the regression analysis includes six variables; three

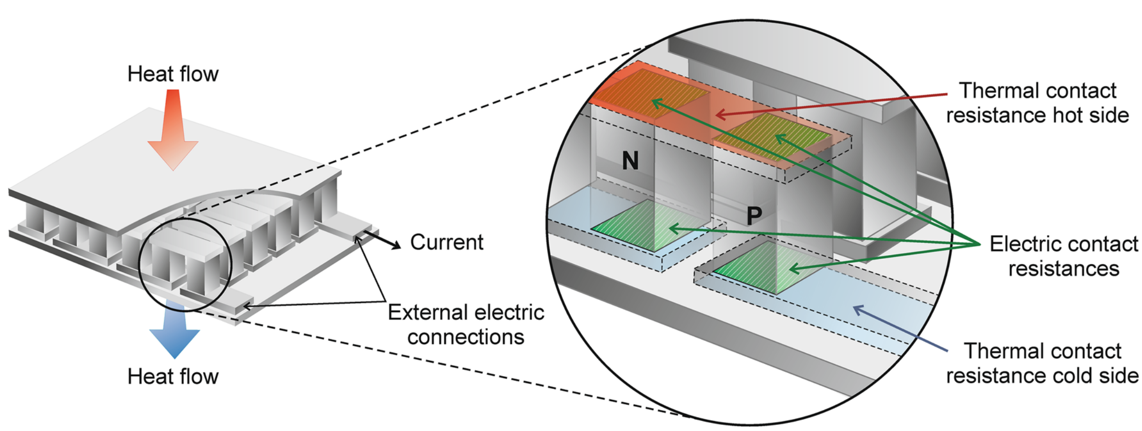

Fig. 2. Contact resistances within the TE modules.

measured and three simulated. Summation of the residuals in the regression analysis requires normalization of the different variables, because the variables have different absolute values and change over the range of operating conditions. Therefore, the sum of squares error is defined as:

$$SS_{\text{reg}} = \sum_{i=1}^{n}\left(\frac{U_i - \hat{U}_i}{U_i}\right)^2 + \sum_{i=1}^{n}\left(\frac{I_i - \hat{I}_i}{I_i}\right)^2 + \sum_{i=1}^{n}\left(\frac{Q_i - \hat{Q}_i}{Q_i}\right)^2, \tag{3}$$

where $\hat{U}, \hat{I}$ and $\hat{Q}$ are the simulated voltage, current, and heat flow, respectively, and the U, I and Q are the corresponding measured response variables. Index i represents the nine different load points in the experiment. Because there are three variables (U, I, and Q) and nine load points, the regression analysis must take a total of 27 observations into account. To determine the values of the model variables, i.e. the contact resistances, they were continuously varied by use of a gradient search method to minimize the total normalized sum of squares. The regression analysis was based solely on the measurements for the large module presented in Table I. The measurement data for the small module, Table II, were used for model validation only.

The regression analysis identified contact resistances that gave very good agreement between simulations and measurements at all nine load points, as shown in Fig. 5. The contact resistances were $\beta_h = 2.0 \times 10^{-4}$ m^2 K W^{-1}, $\beta_c = 1.0 \times 10^{-4}$ m^2 K W^{-1} and $\gamma = 4.8 \times 10^{-9}$ Ω m^2. It should be noted that all the tests were performed at the specified contact pressure of the modules, in this case 1.4 MPa. At this pressure thermal flow and electrical power generation are independent of contact pressure, which was also confirmed by testing. The two thermal contact resistances correspond to reasonably good contact, considering that the contact resistances in the regression analysis were three different resistances in series grouped together. A difference between the thermal contact resistances on the hot and cold sides was expected and can be explained by the design of the module, as already described. The electrical contact resistance was also in the range reported in the literature.

As shown in Fig. 5, the model is capable of predicting voltage, current, and heat flow. The model described module performance very well at all the load points studied, and there was no lack of fit in the model. The R^2 statistics, i.e. the fraction of the total variance around the mean that is explained by the model, were 98.3% for heat flow, 97.5% for current, and 98.7% for voltage. Adjusted R^2 values enable refinement of the statistics because they include a penalty for the number of parameters in the model. The adjusted R^2 values were 98.1% for heat flow, 97.2% for current, and 98.5% for voltage. These values show the model is far from overparameterized, and is therefore reliable.

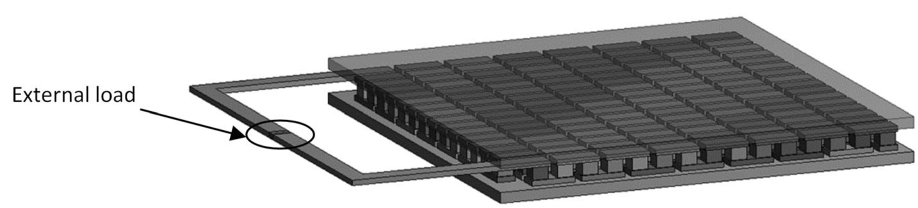

Fig. 3. Simulation model of the thermoelectric module.

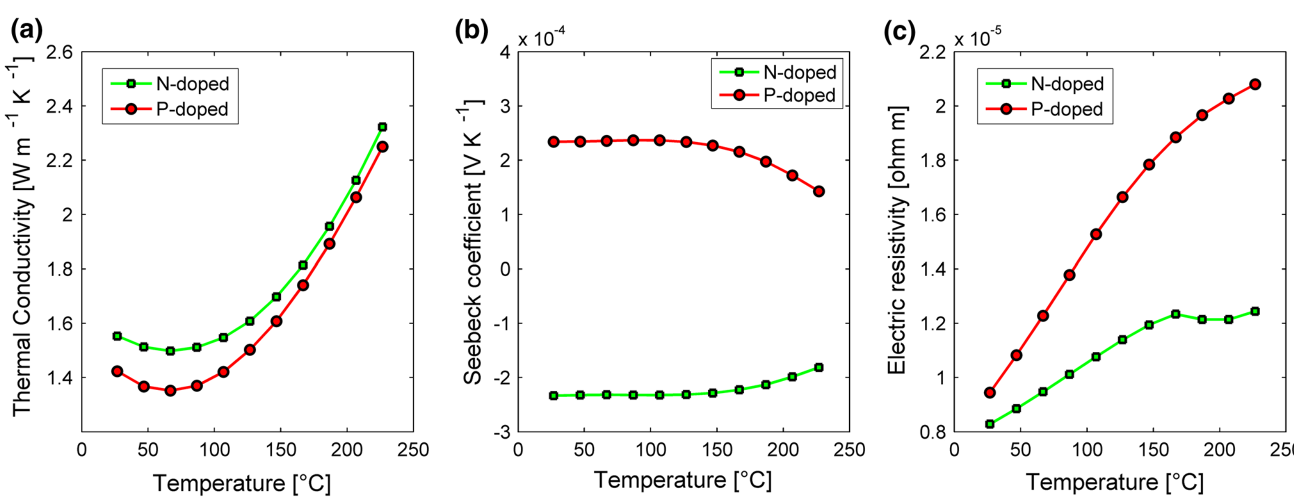

Fig. 4. Material data for Bi_2Te_3 modules: (a) thermal conductivity, (b) Seebeck coefficient, and (c) electric resistivity.

Table II. Measurement data for the small module, TEP1-1264-1.5

Load point	T_h (°C)	T_c (°C)	U (V)	I (A)	Q (W)	P (W)
1	89	21	1.56	0.52	46	0.81
2	118	29	2.22	0.64	56	1.4
3	130	27	2.4	0.72	64	1.7
4	142	26	2.62	0.79	77	2.1
5	159	29	2.9	0.87	81	2.5
6	179	30	3.26	0.96	99	3.1

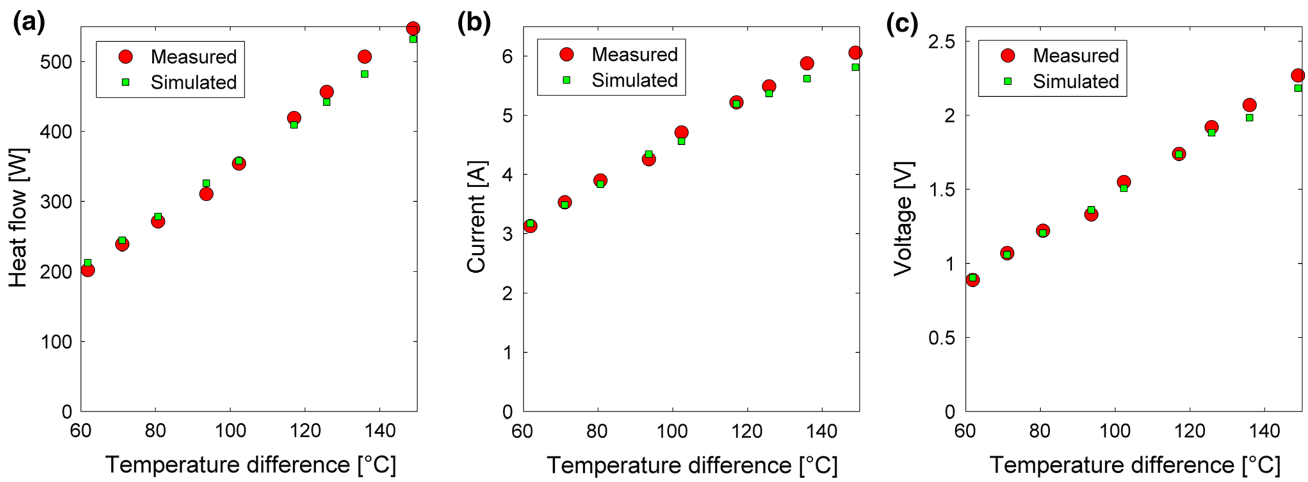

Fig. 5. Measurement and simulation of TEHP1-12680-0.15 with contact resistances: (a) heat flow, (b) current, and (c) voltage.

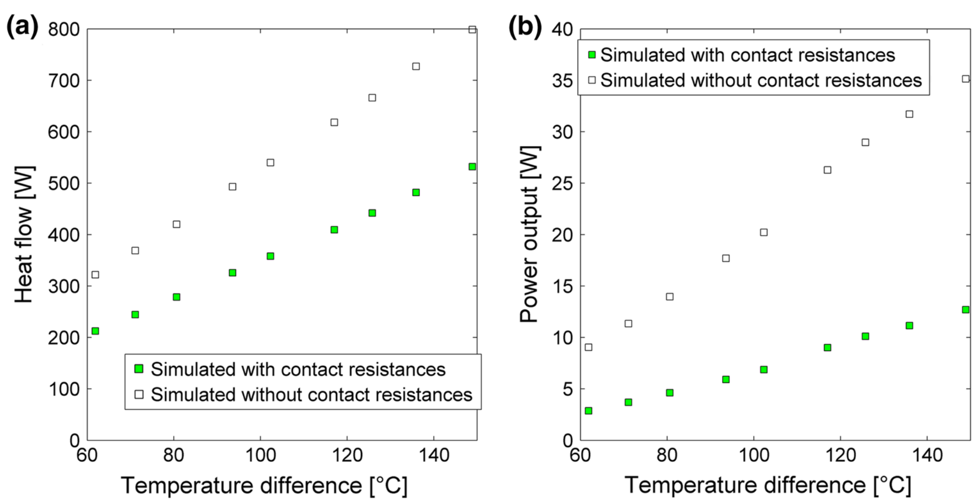

Fig. 6. Comparison of simulations with and without contact resistances: (a) heat flow and (b) electric power output.

The importance of including the contact resistances in the simulations is indicated in Fig. 6, in which simulations with and without contact resistances are compared. It is readily apparent that the contact resistances have a major effect on the simulation performance and should always be included in simulations of modules. If no contact resistances were present, the heat flow and electric power output would be significantly over-predicted, as is apparent from Fig. 6.

To further validate the model and investigate whether the identified contact resistances also enable prediction for geometrically different modules, measurements and simulations were con-

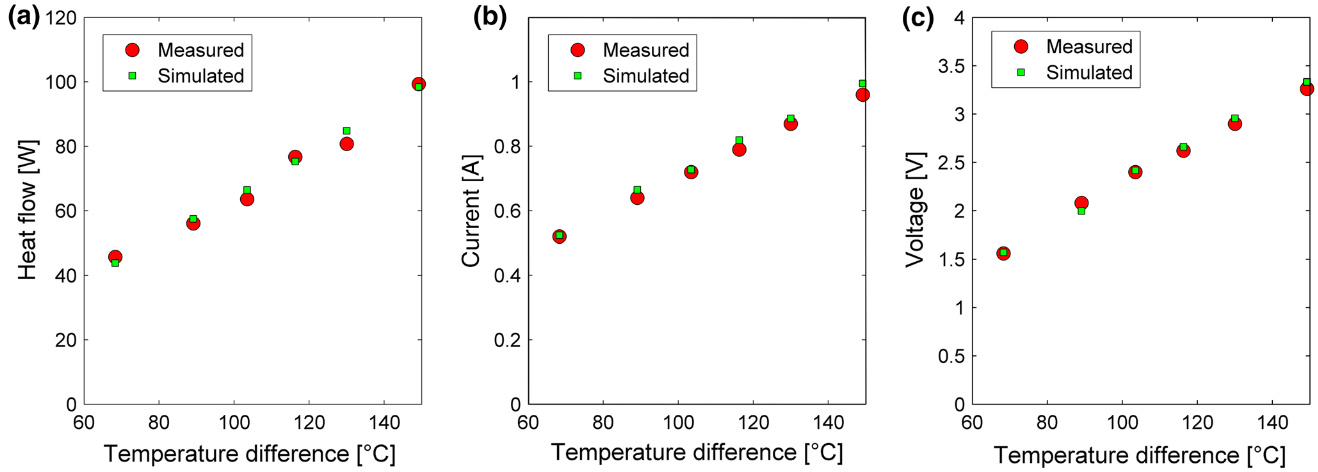

Fig. 7. Measurement and simulation of TEP1-1264-1.5 with contact resistances: (a) heat flow, (b) current, and (c) voltage.

ducted using the small module. The experiments were performed in the same way as described above, under the conditions specified in Table II.

It was concluded that simulations of heat flow, current, and voltage agreed very well with measured data for the small module also. The simulated and experimental results are compared in Fig. 7. The R^2 values for the small module were 97.4% for heat flow, 97.8% for current, and 98.7% for voltage. The corresponding adjusted R^2 values were 96.8% for heat flow, 97.3% for current, and 98.4% for voltage. These values were only slightly lower than those for the large module, and confirm that the model is capable of predicting module performance very well. There was no lack of fit in the model, i.e. there were no systematic deviations between simulated and measured values of voltage, current, and heat flow over the entire operating range. If no contact resistances were present, voltage, current, and heat flow would be significantly over-predicted for this module also. The relative errors of the simulations were approximately the same when contact resistances were excluded from the model.

CONCLUSIONS

In this study 3D finite element modeling was combined with experimental results from commercial TEG Bi_2Te_3-based modules to measure thermal and electrical contact resistances and their effect on module performance. The experimental setup used enabled heat flow, voltage, and current to be measured with high accuracy. Simulations were conducted under the same conditions as in the experiments, i.e., identical heat source and heat sink temperatures and external loads. Non-linear regression analysis was subsequently used to determine contact resistances. The thermal resistances inside the module and on its surfaces were included in two different parameters in the model. Electrical contact resistance was assumed to be identical at all material junctions. This was shown to be sufficient, and enabled highly accurate prediction of module performance, including for modules with different geometrical designs.

Statistical evaluation validated the model and the contact resistances enabled excellent prediction of module performance over the entire range of operating conditions. The question of accuracy of measurement of the contact resistances was addressed by confirming they were also valid for a geometrically different module manufactured by use of the same process and made of the same materials. It was also shown that if no contact resistances were included in the analysis, the simulations systematically over-predicted module performance, by up to 200% for electric power output and approximately 50% for heat flow, even though the contact resistances were moderate and within the range reported in the literature. This also means that the efficiency of the investigated modules, i.e. the ratio of electric power to heat flow, can be increased by minimizing contact resistances.

It was concluded that the methodology presented in this paper enables contact resistances in TEG to be determined accurately, and that the effect of contact resistances should always be taken into account in module simulations. It was, moreover, concluded that this analysis gives detailed insight into how thermoelectric modules perform in general, and enables prediction of potential improvement of module performance by reduction of contact resistances.

ACKNOWLEDGEMENTS

This work was financially supported by the Swedish Foundation for Strategic Environmental Research. The authors would like to thank TermoGen AB for providing equipment for measurements of the modules. The simulations were conducted on the computer cluster at Chalmers University of Technology, supported by the Swedish National Infrastructure for Computing, SNIC.

OPEN ACCESS

REFERENCES

1. G. Fraisse, J. Ramousse, D. Sgorlon, and C. Goupil, *Energy Convers., Manag.* 65, 351 (2013).
2. R. McCarty, *J. Electron. Mater.* 39, 1842 (2010).
3. E.E. Antonova and D.C. Looman, *Finite Elements for Thermoelectric Device Analysis in ANSYS* (New York: IEEE, 2005).
4. Y.A. Cengel and A.J. Ghajar, *Heat and Mass Transfer: Fundamentals & Applications*, 4th ed. (New York: McGraw-Hill, 2011).
5. P. Ziolkowski, P. Poinas, J. Leszczynski, G. Karpinski, and E. Muller, *J. Electron. Mater.* 39, 1934 (2010).
6. M. Chen, L.A. Rosendahl, and T.J. Condra, *Int. J Heat Mass Transf.* 54, 345 (2011).
7. Thermonamic. Ingot specification sheet (Online). www.thermonamic.com. Accessed 18 June 2013.